**Cell**Press

COMMENTARY

# How to Accurately Report Transparent Solar Cells

Chenchen Yang,<sup>1,5</sup>
Dianyi Liu,<sup>1,2,5</sup> Matthew Bates,<sup>1</sup>
Miles C. Barr,<sup>3</sup>
and Richard R. Lunt<sup>1,4,\*</sup>

Chenchen Yang joined the materials science program at Michigan State University in 2015 to work under Prof. Lunt in the Molecular and Organic Excitonics Lab. He earned his B.E. from the University of Electronic Science and Engineering of China in 2012. Then, he obtained his M.S. from University of Florida in 2015. His current research focuses on transparent solar cell synthesis, fabrication, and characterization.

Dianyi Liu obtained his PhD in inorganic chemistry from Lanzhou University in 2009. He then worked as a postdoc at Peking University, the University of Saskatchewan, and Michigan State University. He began as an assistant professor at Westlake University in January 2019. His research interests include flexible electronics, optoelectronic materials, and devices.

Matthew Bates is a graduate student in chemical engineering at Michigan State University working in the Molecular and Organic Excitonic Lab led by Prof. Lunt. He received his B.S. in chemical engineering from Oregon State University in 2016. He is focused on developing transparent photovoltaics.

Miles Barr is co-founder and Chief Technology Officer at Ubiquitous Energy in Redwood City, CA. He earned his bachelor's degree from Vanderbilt University and his Ph.D. from the Massachusetts Institute of Technology, both in chemical engineering. He then co-founded Ubiquitous Energy

and has grown the company through pilot manufacturing, serving as both CEO and CTO. His team is currently working to develop, scale up, and commercialize transparent solar technology for a variety of end applications.

Richard R. Lunt is the Johansen Crosby Endowed Professor at Michigan State University in the Departments of Chemical Engineering & Materials Science and Physics. He earned his B.S. from the University of Delaware and his PhD from Princeton University. He then worked as a post-doctoral researcher at MIT. His group focuses on understanding and exploiting excitonic photophysics and molecular crystal growth to develop unique thinfilm optoelectronic devices. He is known for his pioneering work on transparent solar cells.

### Introduction

Integrating transparent photovoltaics (TPVs) onto new and existing infrastructure as a power-generating source can help to realize net-zero-energy buildings, dramatically improve energy utilization efficiency, and supply on-site energy demand with minimal compromise to the functionality and aesthetic quality of architectural and mobile surfaces. TPV modules can be conveniently installed onto the facades, windows, and siding of buildings as replacements for conventional building materials during construction. Alternatively, they can be directly retrofit onto existing surfaces after initial construction.<sup>1</sup>

Emerging TPV technologies have exhibited tremendous growth in the past 6–7 years. Current TPV technologies can be categorized into two main groups: non-wavelength-selective and wavelength-selective, depending on their corresponding absorption spectra. Non-

wavelength-selective TPVs have exceeded power conversion efficiency (PCE) of 12% with perovskites<sup>2</sup> and  $\sim$ 10% with organic layers with average visible transmittance (AVT) around 20%-30% and light utilization efficiency (LUE =  $PCE \cdot AVT$ ) of 2-3.3 Wavelengthselective TPVs fabricated with organic layers have demonstrated PCEs between 5% and 10% for AVTs between 40% and 55% and LUE of 2.5-4. 1,4,5 theoretical Shockley-Queisser (SQ) limit of a wavelength-selective single-junction TPV with 100% AVT is 20.6%, while the PCE of a non-wavelength-selective TPV approaches 0% as the AVT increases over 90%. Despite the rapid development in TPV research, new characterization challenges have led to less reliable reporting of performance metrics. Thus, it is imperative to adopt standard characterization protocols for these new types of devices, which can provide an unbiased comparison among the reported performance values.6

In this work, we use several example TPVs to comparatively measure all the key performance metrics and consistency checks to highlight the best TPV characterization protocols. We also emphasize common measurement pitfalls, which can lead to inflated performance results. Key parameters to evaluate the visible transparency and aesthetic quality of TPV devices are given along with an overview of the methods to measure and calculate them. Finally, we illustrate the photon balance consistency check for data acquired from independent measurements, which helps validate the data and significantly alleviate concerns over experimental errors.

# Photovoltaic Performance Characterization

The *PCE* of TPVs is defined and calculated exactly the same way as any other PV technology from current density-

**Joule** CellPress

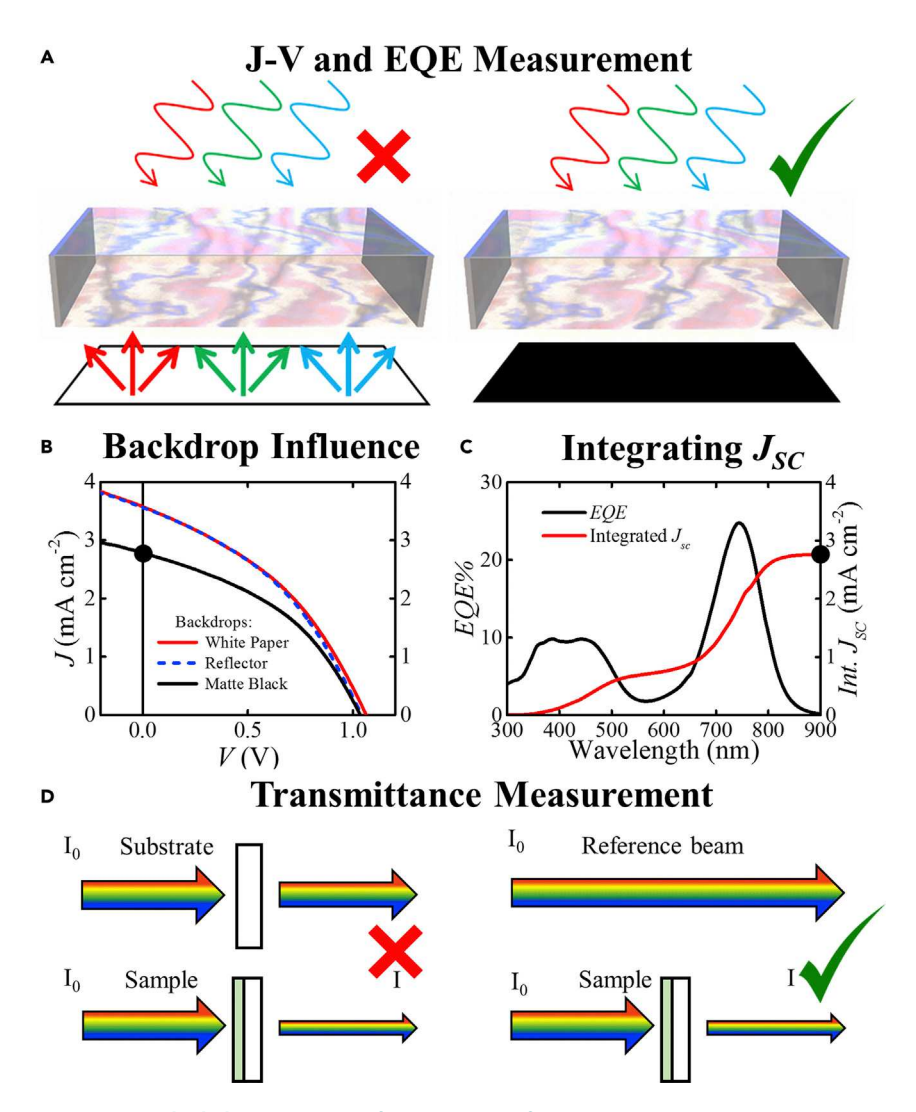


Figure 1. Standard Characterization of TPV Device Performance

(A) Schematic showing the bifacial nature of TPVs that leads to a "double-pass" effect in *J-V* and *EQE* measurements. A matte black backdrop is necessary to avoid overestimation.

(B) J-V characteristic comparison of the same NIR-selective harvesting TPV device using different backdrop conditions. J-V data are measured under simulated AM 1.5G solar illumination (xenon arc lamp with the spectral mismatch factor of 0.97  $\,\pm\,$  0.03).

(C)  $J_{SC}$  integrated from the EQE matches the  $J_{SC}$  extracted from J-V characteristics with the matte black backdrop.

(D) Schematic showing how to measure the transmittance spectra of TPV devices. Note that no reference sample should be utilized in double-beam spectrometers, and the reflectance spectrum should be measured separately.

voltage (*J-V*) characteristics under a standard illumination:

$$PCE = \frac{J_{SC} \cdot V_{OC} \cdot FF}{P_0}$$
, (Equation 1)

where  $J_{SC}$  is the short-circuit current density,  $V_{OC}$  is the open-circuit voltage, and FF is the fill factor. This equation applies to all TPVs and luminescent so-

lar concentrators. We note that the methods for device characterization of luminescent solar concentrators (LSCs) and transparent luminescent solar concentrator (TLSCs) are outlined in our companion article. The incident solar spectrum (P<sub>0</sub>) should always be the AM 1.5G spectrum as the standard input power for both non-wavelength-

selective and wavelength-selective TPV devices. Standard protocols for spatial uniformity of beam illumination, light intensity calibration, and spectral mismatch correction of the solar simulator can be found elsewhere.

Nonetheless, there are still key nuances that are introduced with TPVs compared to traditional opaque cells. Additional consideration for J-V and external quantum efficiency (EQE) measurements of TPVs is required. For example, TPV devices are intrinsically bifacial, which allows illumination from both sides, as shown in Figure 1A. A matte black background should be placed behind the tested device during J-V and EQE measurements to eliminate backside illumination or reflection ("double-pass" effect) from the test environment. In an uncontrolled environment where there is a scattering or reflective surface behind the device, significantly overestimated J-V data can be obtained (see Figure 1B). Additional measurements with different surfaces behind the device (mirrors, scattering layers, etc.) at specified distances can be reported but should supplement (not replace) the standard single-pass measurement. To illustrate the effect of different backdrops on J-V measurements, a single near infrared (NIR)-selective TPV cell with large active area is tested with a masked area of 6.45 cm<sup>2</sup>. Three different backdrop conditions (white paper, broadband reflector, and matte black) are used while testing the J-V characteristics under illumination. All these scans are taken in a darkroom to eliminate contribution from other light sources. The results are shown in Figure 1B, and parameters are summarized in Table S1 (see Note S1). With a white scattering layer or mirror reflector as the backdrop, the measured current densities are nearly 30% higher than the scans with black matte backdrop, which leads to an overestimated overall PCE of 47% from additional  $V_{OC}$  and FFoverestimation. The inflated result



originates from the "double-pass" effect, which is essentially the same in magnitude for either a reflective mirror or a scattering backdrop. For *J-V* measurements, overestimation of the photocurrent can stem from a number of other sources, including mismeasurements of the device area. To alleviate this concern, an opaque mask with a single aperture with well-defined area value should be attached to the PV cell being tested to minimize this photocurrent overestimation (whether there is one or more device on a substrate). <sup>6–8</sup>

One of the first and most important consistency checks for a traditional PV cells is the comparison of the photocurrent density extracted from J-V and from the integrated EQE. The EQE, therefore, should be reported for all TPVs and solar concentrators. This further eliminates concern over photocurrent overestimation. The convolution of the EQE with the AM 1.5G photon flux should match the  $J_{SC}$  from J-V measurements for the same PV device:

$$J_{SC} = \mathbf{e} \cdot \int EQE(\lambda) \cdot AM1.5G(\lambda) d\lambda,$$

(Equation 2)

where e is the elementary charge and  $\lambda$  is the wavelength. The EQE of the same NIR-selective TPV used to compare the influence of the backdrops is shown in Figure 1B, where the integrated  $J_{SC}$  matches that from the J-V measurement with the matte black backdrop. The integrated  $J_{SC}$  from the EQE spectrum should be provided as a consistency check for all future TPV performance reports.

# Figures of Merit for Visible Transparency and Aesthetic Quality

To enable adoption in practical applications (e.g., architectural window glass and mobile surfaces), aesthetics are just as important as *PCE* for TPV devices. Aesthetic quality can be quantitatively evaluated from three main figures

of merit: the AVT, color rendering index (CRI), and CIELAB color coordinates (a\*, b\*). Both the AVT and color coordinates are often the first metrics assessed for many glass, greenhouse, and electronics (display) industries and are utilized as go-no-go criteria for integration (regardless of PCE). The calculation of AVT, CRI, and color coordinates requires the transmittance spectrum of the TPV as input data.1 The addition of this measurement has created substantial confusion and actually requires reporting of both  $T(\lambda)$ and the reflectance spectrum,  $R(\lambda)$ . Historically, solution-based transmittance measurements have utilized solvent-only cuvettes in double-beam spectrometer as a reference to (nearly perfectly) subtract all reflectance and arrive at absorbance spectra (Figure 1D). However, reflections are not so easily referenced from solid films due to complex optical interference and reflections for the tested device compared to reference pieces of glass. Thus, no reference sample should be used for TPV (or thin-films) in doublebeam spectrometers. Reflectance spectra should then be measured separately and reported via direct reflectance measurements from each fully assembled TPV. Reflectance spectra are critical both to the photon balance and as a secondary measure of the CRI and color coordinates (detailed descriptions of  $R(\lambda)$  measurements are described in the Note S2).

We emphasize that when reporting AVT and CRI of any TPV device, the transmittance and reflectance measurements should always be made through the entire device architecture with the beam spot confined within the device area. If the test beam spot is bigger than the device active area, a portion of the incident light can be directly collected by the detector, which can lead to an overestimated  $T(\lambda)$  or an underestimated  $R(\lambda)$ . The best practice is to measure the AVT and PCE on the same device. However, a suitable alter-

native is to test small-area devices for the PCE while using unpatterned larger-area devices for optical measurements, so long as the devices are made side by side. As an example, Figures 2A and 2C shows transmittance spectra of various compositions of halide perovskite active-layer films (1\*-4\*), 10 NIR-selective harvesting active-layer films (5\*-7\*), and complete TPV devices (1-4 for perovskite PVs and 5-7 for NIR-selective harvesting PVs). We emphasize that there is a significant difference in the transmittance spectra between the film and complete PV devices due to additional reflectance and optical interference.

AVT (also commonly referred to as visible transmittance, "VT," or visible light transmittance, "VLT") is independent of any defined visible wavelength range and relies solely on the photopic response of the human eye. Examples of AVT calculations are provided in Note S3. This is also the definition long utilized by the window industry and recently introduced into the PV community.<sup>11</sup> The transmitted photon flux (AM 1.5G  $\cdot$   $T(\lambda)$ ) and  $V(\lambda)$  are plotted in Figure 2B for both perovskite and NIR-selective PVs and illustrate that both the shape and absolute value of  $T(\lambda)$  can affect how the incident photon flux is attenuated (especially for wavelengths where  $V(\lambda)$  is largest) and thus impacts the AVT. Photographs of various compositions of halide perovskite active-layer films, different NIR harvesting active-layer films, and the corresponding TPVs are also shown in the inset of Figures 2A and 2C. An important metric that should be reported is the LUE, which is the product of AVT and PCE. The LUE provides a metric for comparing TPVs with different overall levels of AVT on the same scale. The LUE limits are 20.6% and 36.6% for single-junction and multijunction TPVs with 100% AVT, respectively. 11 Reporting LUE enables a fair performance comparison between different TPV technologies and

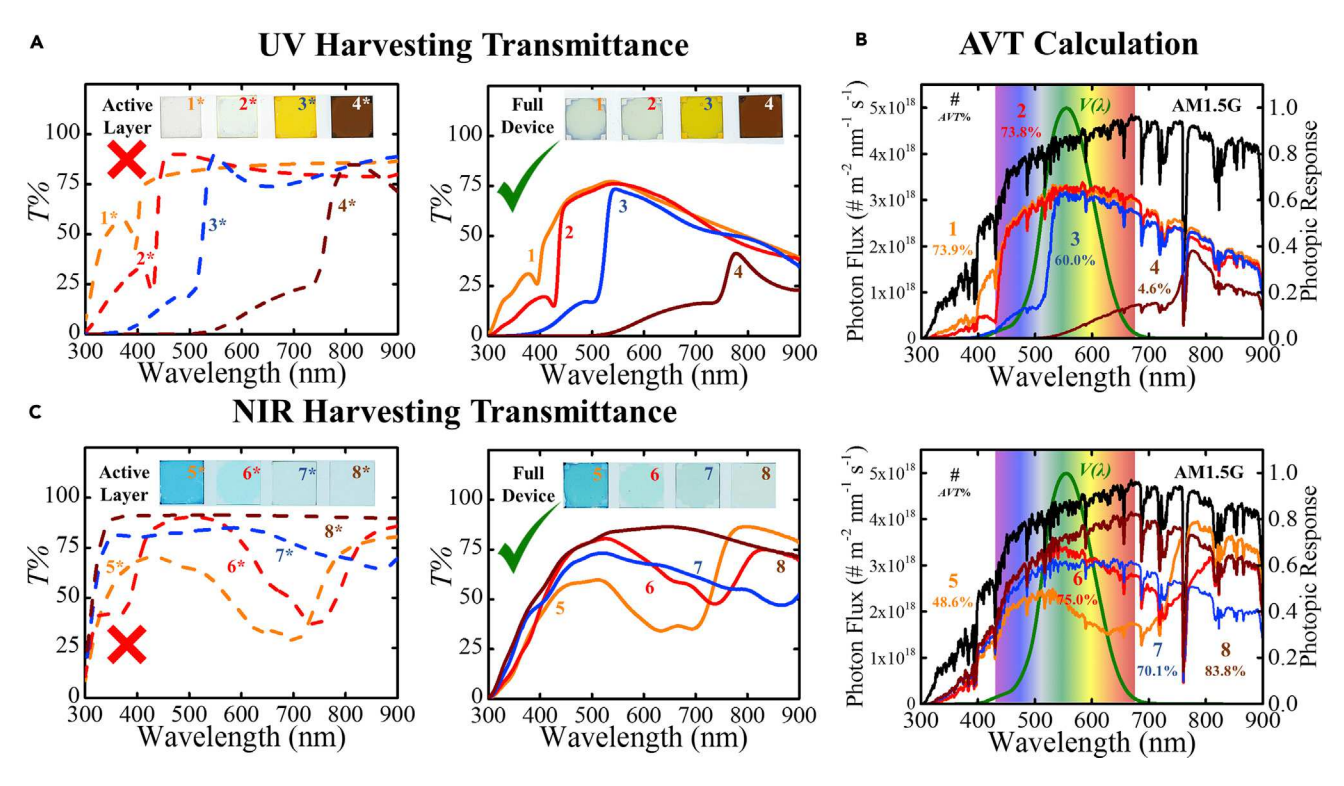


Figure 2. Transmittance Spectra and Average Visible Transmittance

(A) Transmittance spectra of various UV and blue-absorbing perovskite active-layer films with different composition (1\*-4\*) and complete perovskite TPV devices (1-4). Inset: photograph of the corresponding films or devices.

(B) AM 1.5G photon flux, transmitted photon fluxes through PV devices 1–8, and photopic response function  $V(\lambda)$ . We note that photon flux should be utilized for the AVT calculation.

(C) Transmittance spectra of various NIR-red-absorbing active-layer films (5\*–7\*; 8\* is the glass substrate) and devices (5–7 are complete devices, and 8 does not have an active layer). Device 8 is fabricated to show the impact on the TPV transmittance from carrier transport layers and electrodes. Inset: images of the corresponding films and devices photographed in transmission mode.

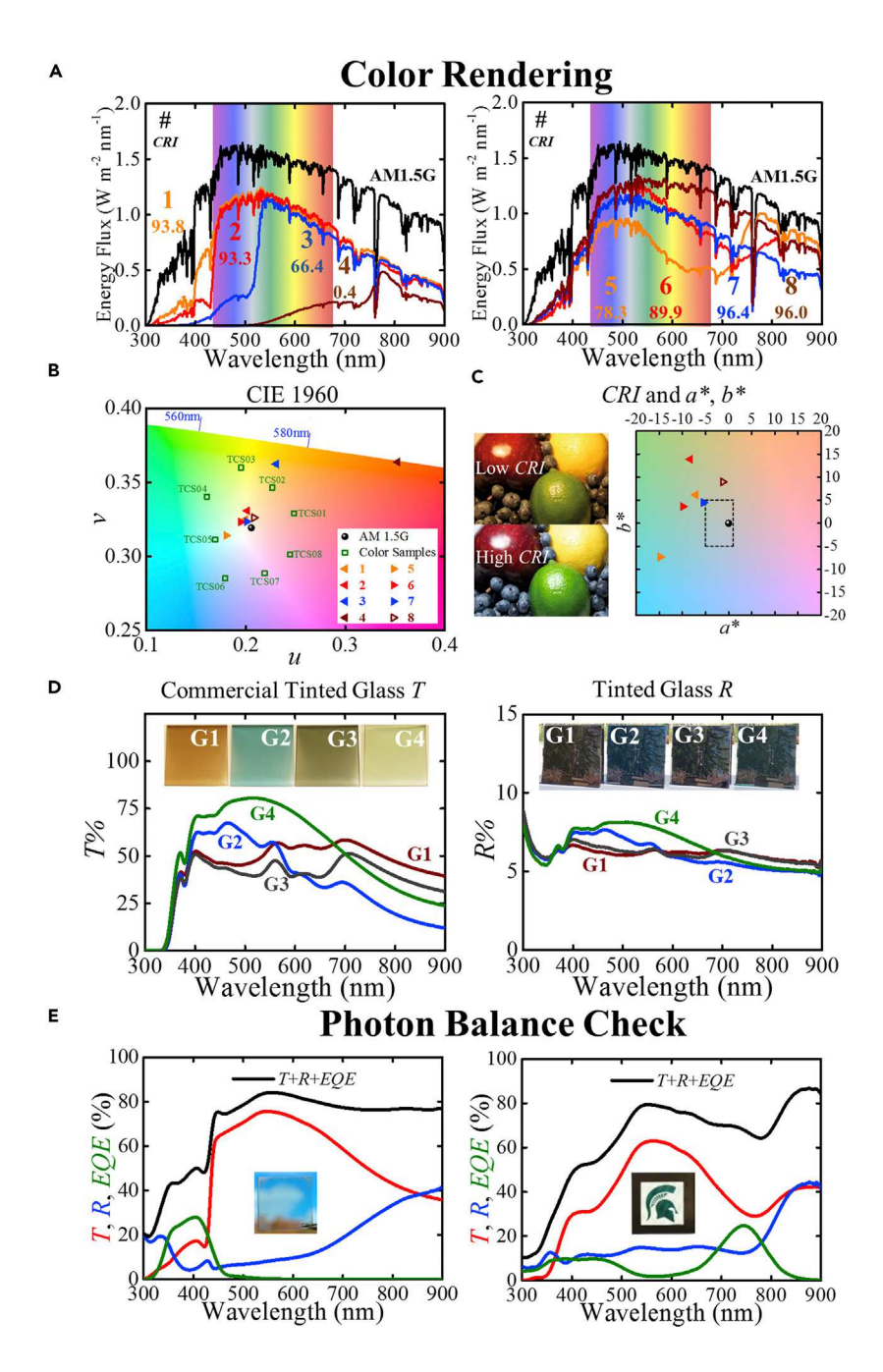
theoretical limits, which can be used as a metric to evaluate the ability of a TPV technology to simultaneously optimize both visible transparency and power conversion, track the best utilization of light, and assess progress in the field.<sup>1</sup>

In addition to the AVT, two key figures of merit for TPV aesthetics that should be reported are the CRI and CIELAB color space parameter set (a\*, b\*), which quantify the rendered color fidelity of objects from a test light source and indicate relative color with respect to a reference illumination source. However, in applying this analysis to TPVs, there are nuances that need to be noted. In particular, it is a combination of both color coor-

dinates and CRI that define the acceptable range of optical properties for window applications. Detailed descriptions of CRI calculations can be found in Note S4. AM 1.5G has been used as the test standard for incident power since the 1970s, and it is therefore the AM 1.5G energy flux that should always be the reference spectrum for CRI calculation in TPV applications (additional spectrum, e.g. the spectra of a backlit display, can also be utilized in these calculations as a supplement for display mounted TPVs). The AM 1.5G and transmitted energy fluxes (AM  $1.5G \cdot T(\lambda)$ ) for various PVs (devices 1-8) are plotted in Figure 3A as the "reference source" and "test sources" power spectra.

A comparison of objects illuminated with low and high CRI light sources is shown in Figure 3C (left). We note that CRI is not a function of AVT but rather the shape of the spectrum through the visible (i.e., it is possible to have an AVT of 10% and a CRI of 100 if the transmittance spectrum is flat through the visible). Transmittance and reflectance spectra of several commercial tinted glass samples are plotted in Figure 3D and the  $(a^*, b^*)$  values are tabulated in Table S2 (Note S5). In the window industry, CRI is applied to evaluate the ability of portraying a variety of colors of the transmitted daylight through glazing compared to those observed directly under daylight without the glazing. Threshold values for the CRI in the window industry actually depend





on the position of the color coordinates described below.

The CIELAB color space coordinates (a\*, b\*) (Figure 3C [right]) are typically the first metric utilized to assess acceptable ranges of color tinting for mass-market architectural glass products. While u and v are used to calculate CRI, we recommend reporting a\* and b\* to characterize position in the color space, which is the standard in the window industry. On this scale,  $a^*$  and  $b^*$  at the origin (0, 0) is colorless. The color coordinate box that defines the region of acceptable tinting for many mass-market architectural glass products is  $-5 < a^* < 1$  and  $-5 < b^* < 5$ . Tinted glass with values near the origin (neutral or gray) or negative values of a\* (greenish) and negative b\* (bluish) are found to be more visually acceptable for modern window deployment than positive values of a\* (reddish) and positive b\* (yellowish). CRI is interdependent with  $a^*$  and  $b^*$ , as all parameters are defined by the same transmission spectrum; therefore, the CRI threshold requirements for one corner of the acceptable color coordinate box will differ from the CRI requirements in other regions. For example, blue-tinted coatings (i.e., negative a\* and  $b^*$ ) only require CRI > 90 because the color of the tint is more acceptable, whereas the less desirable yellow- or red-tinted coating (e.g., a\* or b\* close to 0 or positive) requires higher CRI > 95 to remain in an acceptable color range. For this reason, it is imperative that both values are reported. Similar considerations can also be applied to

Figure 3. Color Rendering and Photon Balance

(A) AM 1.5G energy flux and transmitted energy fluxes of PV devices 1–8. We note that it is energy flux that should be utilized for *CRI* calculations based on the construction of the *CRI* formalism. Note that as the UV absorption cutoff increases beyond 430 nm or the NIR absorption peaks decreases below 675 nm, the *CRI* drops quickly, as outlined in Table S2, resulting in strongly tinted films and devices.<sup>2</sup> On the UV side, this leads to positive values of (b\* or a\*), while on the NIR side, this leads to negative values (b\* or a\*), where modestly negative values of a\* and b\* are more acceptable to the window industry.

(B) CIE1960 color space used to calculate CRI with test color samples (TCS01–TCS08) and PV devices 1–8. AM 1.5G is also included as the "reference light source."

(C) Comparison of objects illuminated by high and low *CRI* light source (left): under low *CRI* conditions; for example, blueberries look like blackberries. CIELAB color space (right): the dashed box illustrates the region of acceptable tinting for many mass-market architectural glass products. Note: PV devices 3 and 4 are strongly tinted in visible and their corresponding (a\*, b\*) coordinates are outside of the shown scale.

(D) T and R spectra of commercial tinted glass sheets: bronze (1), blue (2), grey (3), and green (4). A summary of CRI and a\*b\* values are provided in Table S2. Inset: photographs of the transmitted and reflected color of C1–C4 glass samples.

(E) Photon balance check for a UV-selective harvesting (left) and NIR-selective harvesting TPVs (right). Inset: photographs of the corresponding TPV devices.



reflected color, and both transmission and reflection effects should be taken into account to compose representative photographs for publication (see Note S6). To aid in the assessment of AVT, CRI, and (a\*, b\*), we provide a spreadsheet in the Supplemental Information that calculates these parameters based on an input T or R spectra. Thus, these parameters should also be provided in all TPV reports.

### **Measurement Validation**

In addition to the integrated  $J_{SC}$  consistency check described above, the photon balance (at every wavelength) should be used to check all key TPV devices:

$$A(\lambda)+R(\lambda)+T(\lambda)=1$$
, (Equation 3) where  $A(\lambda)$  is the absorption spectrum of the entire TPV device. However, since it is difficult to directly measure  $A(\lambda)$ , and  $EQE(\lambda) \leq A(\lambda)$ , we can take the limit of internal quantum efficiency  $IQE(\lambda) \leq 1$  (unless multiple exciton generation [MEG] exists) so that the following relation should be satisfied at every wavelength with independent measurements of  $EQE(\lambda)$ ,  $T(\lambda)$ , and

 $EQE(\lambda) + R(\lambda) + T(\lambda) \le 1$ . (Equation 4)

In the case that MEG is present, the EQE term in Equation 4 must be replaced with EQE per IQE, where IQE is the internal quantum efficiency. In the case of multijunction devices, the IQE is reduced in exchange for an increase in output voltage (multiple absorbed photons generate one electron-hole pair to obtain higher potential) so that the EQE in Equation 4 should be replaced by the summation of the EQE spectrum of all sub-cells. Thus, the photon balance consistency check should be applied to every type of TPV. Two examples of this simple consistency check are shown for both UV- and NIR-selective harvesting TPVs in Figure 3E. We note that this balance per IQE) in the same report, provided Equation 4 is still shown to be met. We also encourage reporting of parasitic losses (e.g., parasitic absorption losses from transport layers and electrodes), as outlined in Xia et al., <sup>13</sup> whenever possible. At a minimum, all reports on TPVs should provide independent  $EQE(\lambda)$ ,  $T(\lambda)$ , and  $R(\lambda)$  measurements and provide such validation checks for each emphasized device to minimize potential experimental errors.

#### Conclusion

Various emerging TPV technologies provide a compliment to traditional PVs to help meet the growing energy demand of the world. A rapid increase in TPV reports indicates excitement for this emerging field. However, a misunderstanding of the measurements needed to characterize these new devices and the target metrics for widespread adoption has created substantial confusion in the literature. In this work, standard protocols of TPV characterization are clearly outlined and common pitfalls are described. While the PCE for TPVs should be measured in similar fashion to the opaque counterparts, there are additional nuances to their measurement. Further, we discuss the additional measurements required for characterizing TPV devices. AVT, CRI, and a\*, b\* are critical figures of merit that are as important as PCE and EQE, if not more so. We describe how to accurately measure and report AVT, CRI, and (a\*, b\*) metrics, outline key targets for these properties in the window industry, and show these calculations for a number of TPV materials and devices. In addition, the photon balance is used as a tool to validate independent spectral measurements of EQE, transmittance, and reflectance. This work outlines necessary approaches for characterizing and reporting TPVs, which are an exciting new paradigm for PV research that can enable new opportunities and new applications for solar energy harvesting.

## SUPPLEMENTAL INFORMATION

Supplemental Information can be found online at https://doi.org/10.1016/j.joule. 2019.06.005.

# **ACKNOWLEDGMENTS**

The authors gratefully acknowledge support from the National Science Foundation under grant CBET-1702591.

## **DECLARATION OF INTERESTS**

M.C.B. and R.R.L. are cofounders of Ubiquitous Energy Inc., a company working to commercialize transparent photovoltaics.

- 1. Traverse, C.J., Pandey, R., Barr, M.C., and Lunt, R.R. (2017). Emergence of highly transparent photovoltaics for distributed applications. Nat. Energy 2, 849–860.
- Yuan, L., Wang, Z., Duan, R., Huang, P., Zhang, K., Chen, Q., Allam, N.K., Zhou, Y., Song, B., and Li, Y. (2018). Semitransparent perovskite solar cells: unveiling the trade-off between transparency and efficiency. J. Mater. Chem. A 6, 19696– 19702.
- Liu, F., Zhou, Z., Zhang, C., Zhang, J., Hu, Q., Vergote, T., Liu, F., Russell, T.P., and Zhu, X. (2017). Efficient semitransparent solar cells with high NIR responsiveness enabled by a small-bandgap electron acceptor. Adv. Mater. 29, 1606574.
- Wang, W., Yan, C., Lau, T.K., Wang, J., Liu, K., Fan, Y., Lu, X., and Zhan, X. (2017). Fused hexacyclic nonfullerene acceptor with strong near-infrared absorption for semitransparent organic solar cells with 9.77% efficiency. Adv. Mater. 29, 1701308.
- Ubiquitous energy certifies new world record performance for transparent solar cell. https://www.businesswire.com/news/ home/20190320005019/en/Ubiquitous-Energy-Certifies-New-World-Record-Performance.
- Zimmermann, E., Ehrenreich, P., Pfadler, T., Dorman, J.A., Weickert, J., and Schmidt-Mende, L. (2014). Erroneous efficiency reports harm organic solar cell research. Nat. Photonics 8, 669–672.
- Snaith, H.J. (2012). How should you measure your excitonic solar cells? Energy Environ. Sci. 5, 6513–6520.
- Snaith, H.J. (2012). The perils of solar cell efficiency measurements. Nat. Photonics 6, 337–340.
- Shrotriya, V., Li, G., Yao, Y., Moriarty, T., Emery, K., and Yang, Y. (2006). Accurate measurement and characterization of organic solar cells. Adv. Funct. Mater. 16, 2016–2023.

 $R(\lambda)$ :<sup>1</sup>

can also be used to estimate the IQE

(replacing EQE in Equation 4 with EQE

Please cite this article in press as: Yang et al., How to Accurately Report Transparent Solar Cells, Joule (2019), https://doi.org/10.1016/j.joule.2019.06.005

# **Joule**



- Liu, D., Yang, C., and Lunt, R.R. (2018). Halide perovskites for selective ultravioletharvesting transparent photovoltaics. Joule 2, 1827–1837.
- 11. Lunt, R.R. (2012). Theoretical limits for visibly transparent photovoltaics. Appl. Phys. Lett. 101, 43902.
- 12. International Glazing Database. https://windows.lbl.gov/software/igdb.
- Xia, R., Gu, H., Liu, S., Zhang, K., Yip, H.-L., and Cao, Y. (2019). Optical analysis for semitransparent organic solar cells. Sol. RRL 3, 1800270.
- <sup>1</sup>Department of Chemical Engineering and Materials Science, Michigan State University, East Lansing, MI 48824, USA
- <sup>2</sup>School of Engineering, Westlake University, 18 Shilongshan Road, Hangzhou 310024, China
- $^{3}$ Ubiquitous Energy, Inc., Redwood City, CA 94063, USA
- <sup>4</sup>Department of Physics and Astronomy, Michigan State University, East Lansing, MI 48824, USA
- $^{5}\mbox{These}$  authors contributed equally
- \*Correspondence: rlunt@msu.edu

https://doi.org/10.1016/j.joule.2019.06.005